THE JOURNAL OF PHYSICAL CHEMISTRY B

Article

pubs.acs.org/JPCB

Polarizable Force Field with a σ-Hole for Liquid and Aqueous Bromomethane

Archita N. S. Adluri,[†,‡] Jennifer N. Murphy,[†,‡] Tiffany Tozer,[†,‡] and Christopher N. Rowley*[,†]

[†]Department of Chemistry, Memorial University of Newfoundland, St. John's, Newfoundland A1B 3X7, Canada

Supporting Information

ABSTRACT: Bromomethane (CH_3Br) is an acutely toxic environmental pollutant that contributes to ozone depletion. Molecular simulation could be a valuable tool for studying its partitioning and transport in the environment if an accurate molecular model was available. The generalized Amber force field (GAFF), OPLS (optimized potentials for liquid simulations) force field, and CHARMM general force field (CGenFF) were tested for their ability to model the physical properties of liquid bromomethane. The OPLS force field was in fairly good agreement with experiment, while CGenFF and GAFF were significantly in error. The Br Lennard-Jones parameters of the GAFF and CGenFF models were reparameterized, but their radial distribution functions still have significant deviations from those calculated by ab initio molecular dynamics (AIMD). A Drude polarizable force field for bromomethane was parametrized with an off-center positively charged site to represent the C−Br σ-hole. This model is in good agreement with the bulk physical properties and the AIMD RDFs. The modest solubility of bromomethane was reproduced by this model, with dispersion interactions being the dominant water−solute interaction. The water−solute electrostatic interactions are a smaller factor in solubility. This model predicts bromomethane to have a 13 kJ mol^{-1} surface excess potential at the water−vapor interface.

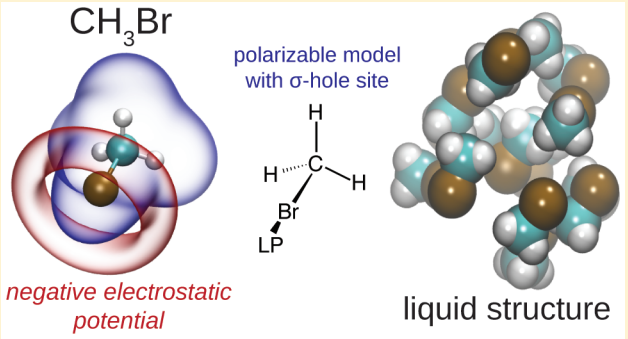

INTRODUCTION

Bromomethane is used extensively as a fumigant and fungicide. This compound exhibits acute and chronic toxicity.[1] Bromomethane photodegrades to form a bromine radical that can catalyze the decomposition of ozone.[2] This ozone-depleting character has resulted in increased regulation of its agricultural and industrial use. Bromomethane is also produced in significant amounts by vegetation in the ocean,[3] wetlands,[4] and salt marshes,[5] so global atmospheric models include both natural and anthropogenic sources.[6]

Atomistic computer simulation can be a valuable tool for understanding the behavior of environmental pollutants.[7−11] This type of modeling is particularly useful for species where experimental data are not available or are unreliable. An effective molecular model for bromomethane would make it possible to simulate its partitioning and transport in aqueous environments. This is significant because the ocean is both the largest sink and the largest source in the atmospheric budget for bromomethane.[6] The concentration of bromomethane in the surface−microlayer, its rate of diffusion in water, and its solvation in water are all significant for understanding its environmental impact.

Several general-purpose force fields include parameters for brominated compounds. The generalized Amber force field (GAFF),[12] OPLS (optimized potentials for liquid simulations),[13] and CHARMM general force field (CGenFF)[14] are general-purpose force fields that have bonded and nonbonded parameters for the Br atom type. A recent study of the accuracy of the GAFF and CGenFF for calculating the physical properties of molecular liquids showed that these force fields performed well for many molecular liquids that were tested but performed poorly for bromomethane.[15] Both models underestimate the density and enthalpy of vaporization of liquid bromomethane.

There are several possible causes for the failure of these models. There are a limited number of brominated compounds in the target data used in the parametrization of these models, so the default parameters may not be optimal. The failure could also be due to approximations inherent to those models. One of the most significant approximations of these models is the use of fixed charges at the nuclear centers to describe electrostatic interactions. Organobromides exhibit a σ-hole effect, which results in a depletion of charge density on the side of the bromine atom opposite to the C−Br σ bond.[16−22] Conventional generalized force fields only use nuclear-centered charges, so this effect is neglected. These charges are constant, so induced electron polarization is also neglected. This effect

Received: September 16, 2015
Revised: September 27, 2015
Published: September 30, 2015

DOI: 10.1021/acs.jpcb.5b09041
J. Phys. Chem. B 2015, 119, 13422−13432

could be significant because bromomethane has a high polarizability (α = 5.6 Å^3).[23]

The σ-hole effect has been successfully incorporated into molecular mechanical models by adding off-center charges. These "lone pair" sites are massless, charged particles that are constrained to positions with respect to the atomic centers. Using these particles, the effect of a σ-hole can be approximated by placing a positively charged site on the side of the halogen, opposite to the σ-bond (i.e., collinear to the C−X bond axis).[24−26]

Polarizability can be incorporated into molecular mechanical models through a variety of methods. Mu et al. successfully used a polarizable multipole force field to describe organochloride species.[27] The Drude model is an alternative polarizable model that provides a simple and computationally efficient scheme for including the effects of induced polarization within existing molecular mechanical codes.[28,29] This method has been successfully used to describe water,[30,31] ions,[32−35] amides,[36] alkanes,[37] sulfur-containing compounds,[7,38,39] lipid bilayers,[40,41] carbohydrates,[42] nucleic acids,[43−46] and proteins.[47] Although bromine is a highly polarizable atom, to date, Drude force field parameters for bromine substituents have not been reported.

An additional challenge in the development of an improved molecular model for bromomethane is that there is no reported experimental neutron or X-ray scattering data on the liquid structure. The structure factor curves determined from this type of experiment can be used evaluate the accuracy of pair-correlation functions of the simulated liquid structure. In the absence of experimental scattering data, ab initio molecular dynamics can provide a first-principles estimate of these distributions.[48] This method allows a small unit cell of the liquid to be simulated using a quantum chemical method (e.g., DFT). This provides a secondary check on the ability of the model to predict the liquid structure, independent of the bulk physical properties the model is parametrized for.

In this paper, we present the results of molecular dynamics simulations of bromomethane using the GAFF, CGenFF, and OPLS general nonpolarizable force fields. We compare the results of these simulations with the experimental properties of the liquid and the AIMD radial distribution functions. We then reoptimize the GAFF and CGenFF Br Lennard-Jones parameters to improve the accuracy of these models. To improve the model further, we develop a Drude polarizable force field and use this model to study the solvation of bromomethane in liquid water.

THEORY AND METHODS

Force Fields. Standard parameters were used for the simulations with the general nonpolarizable force fields. The charges for the GAFF model were assigned using the restrained electrostatic potential (RESP) method to fit to the HF/6-31G*electrostatic potential surface. CGenFF parameters[49] were assigned using the MATCH program.[50] OPLS parameters[13] were taken from the Virtual Chemistry database entry for bromomethane.[15] The parameter and topology files for these models are included in the Supporting Information.

These force fields have a common potential energy expression. Bond and bond angle internal energy terms are described by harmonic potentials

$$U_{\text{bonded}} = \sum_{i}^{\text{bonds}} k_{\text{bond},i}(r_i - r_{0,i})^2 + \sum_{i}^{\text{angles}} k_{\text{angle},i}(\theta_i - \theta_{0,i})^2 \quad (1)$$

The Drude model incorporates the effect of polarizability by harmonically tethering an additional positively charged particle to each non-hydrogen atom.[28,51] Intermolecular 1−2 and 1−3 electrostatic interactions are screened by a Thole function.[52] All other electrostatic interactions are calculated using standard expressions for pairwise point-charge−point-charge interactions. The total nonbonded interactions are calculated as the pairwise sum of the Coulombic interaction and Lennard-Jones potential over all nonbonded pairs of the N atoms in the system

$$U_{\text{nonbonded}} = \sum_{A}^{N}\sum_{B>A}^{N} \frac{1}{4\pi\epsilon_0}\frac{q_A q_B}{r_{AB}} + \sum_{A}^{N}\sum_{B>A}^{N} 4\varepsilon_{AB}\left[\left(\frac{\sigma_{AB}}{r_{AB}}\right)^{12} - \left(\frac{\sigma_{AB}}{r_{AB}}\right)^{6}\right] \quad (2)$$

where r is the interatomic distance between atoms A and B. The Lennard-Jones parameters (σ and ε) for unlike pairs were calculated using the Lorentz−Berthelot combination rules[53,54]

$$\sigma_{AB} = \frac{\sigma_{AA} + \sigma_{BB}}{2},\ \varepsilon_{AB} = \sqrt{\varepsilon_{AA}\varepsilon_{BB}} \quad (3)$$

MD Simulation Details. The simulations of the nonpolarizable models were performed using NAMD 2.10.[55] The simulations of the Drude polarizable model were performed using CHARMM c38b2.[56] Electrostatic interactions were calculated using the particle mesh Ewald (PME) method[57] with a 1 Å grid spacing. Lennard-Jones interactions were calculated using a smoothed cutoff potential between 12 and 16 Å. The C−H bonds were constrained to 1.111 Å using the SHAKE algorithm.[58] A Langevin thermostat was used with a damping coefficient of 1 ps^{-1}. Isothermal−isobaric NAMD simulations used a Langevin piston barostat,[59] while CHARMM simulations used an Anderson-Hoover barostat.[60] Simulations of the nonpolarizable systems used a 2 fs time step. Simulations using the Drude model used a 1 fs time step because of the small mass of the Drude particles.

Ab Initio Molecular Dynamics. AIMD simulations of bromomethane were performed using CP2K version 2.3.[61] The simulation was performed in the canonical (NVT) ensemble with a density corresponding to the experimental value. The cubic unit cell had dimensions of 16.3 × 16.3 × 16.3 Å containing 55 CH_3Br molecules. The PBE functional[62] with the Grimme D3 correction for dispersion[63] was used. The DZVP basis set and Goedecker-type pseudopotentials were used to describe all atoms.[64] The C−H bonds were constrained to a distance of 1.11 Å. The mass of the Br atoms was reduced to 12 u to allow for more rapid sampling of the liquid configurational space. The system was propagated using Langevin dynamics with a 1 fs time step and a friction coefficient of 1 ps^{-1} at a temperature of 276 K. The system was initiated from an equilibrated configuration from a simulation using the OPLS model. A 20 ps equilibriation was performed prior to a 100 ps production simulation.

Ab Initio Dimerization Energy. The dimerization energy of bromomethane was calculated by performing a geometry optimization on the dimeric structure using counterpoise-corrected[65] MP2/aug-cc-pVTZ in Gaussian 09.[66] The dimeri-

DOI: 10.1021/acs.jpcb.5b09041
J. Phys. Chem. B 2015, 119, 13422−13432

Table 1. Parameters and Calculated Properties of Liquid Bromomethane (T = 276 K, p = 101.325 kPa) for the General Nonpolarizable Models[a]

property	GAFF	CGenFF	OPLS	exptl
σ_{Br} (Å)	1.7996	1.7551	1.735	
ϵ_{Br} (kJ mol^{-1})	1.7577	2.0088	1.9669	
q_{Br} (e)	−0.124661	−0.10	−0.22	
μ_0 (D)	2.17	1.402	2.52	1.797 ± 0.015[b]
E_{dimer} (kJ mol^{-1})	−10.7	−7.5	−12.5	−10.3[c]
ρ (kg m^{-3})	1659.1 ± 1.0	1635.7 ± 2.5	1732.2 ± 0.5	1722.0[d]
ΔH_{vap} (kJ mol^{-1})	20.71 ± 0.01	16.71 ± 0.02	24.99 ± 0.01	24.1[e]
γ (dyn/cm)	17.3 ± 2.7	18.1 ± 0.8	23.6 ± 0.04	27.3[f]
ϵ_0	7.87 ± 0.13	3.54 ± 0.04	11.8 ± 0.36	9.82[g]

[a]Experimental values are given in the rightmost column. [b]Reference 79. [c]CCSD(T)/aug-cc-pVTZ//MP2/aug-cc-pVTZ. [d]Reference 80. [e]Reference 81. [f]Reference 82. [g]Reference 83.

zation energy of this optimized structure was calculated using TURBOMOLE 7.0[67] using RI-CCSD(T)[68] with the aug-cc-pVTZ basis set.[69] A counterpoise correction was also performed in the CCSD(T) calculation.

Physical Properties. The density (ρ), enthalpy of vaporization (ΔH_{vap}), and dielectric constants (ϵ) of the models were calculated from isothermal−isobaric molecular dynamics simulations of the neat liquid. A 32 × 32 × 32 Å unit cell of bromomethane was constructed using the Liquefy plugin of VMD.[70] A 1 ns NpT molecular dynamics simulation was performed to equilibrate the system. Averages were then calculated from 10 ns NpT molecular dynamics simulations. Where the uncertainty of a value is reported, the simulation was repeated 3 times and the averages and standard deviations of the results of these simulations are reported.

The dielectric constant of liquid bromomethane was calculated using the relation[71]

$$\epsilon = \epsilon_\infty + \frac{4\pi(\langle M^2\rangle - \langle M\rangle^2)}{3\langle V\rangle k_B T} \quad (4)$$

In this equation, M is the dipole moment of the unit cell, $\langle V\rangle$ is the volume of the cell, and ϵ_∞ is infinite frequency dielectric constant, which is equal to 1 for the nonpolarizable models but can exceed this value in polarizable models. For the Drude model, this term was estimated using the Clausius−Mossotti equation

$$\frac{\epsilon_\infty - 1}{\epsilon_\infty + 2} = \frac{4\pi\alpha}{3\nu} \quad (5)$$

where α is the calculated molecular polarizability and ν is the molecular volume.

The surface tension (γ) was calculated from the pressure tensor averages of an isothermal−isochoric simulation of a 22.51 × 22.51 × 22.51 Å slab of 125 CH_3Br molecules in a 22.51 × 22.51 × 64 Å unit cell using the relation

$$\gamma = \frac{1}{2}L_z\left[\langle P_{zz}\rangle - \frac{1}{2}(\langle P_{xx}\rangle + \langle P_{yy}\rangle)\right] \quad (6)$$

where P_{ii} are the diagonal elements of the pressure tensor and L_z is the length of the unit cell along the z axis. The surface was equilibriated for 1 ns. Averages of the pressure tensor elements were calculated from 10 ns simulations.

Solvation Properties. *Gibbs Energy of Hydration.* The Gibbs energy of hydration was calculated using a decoupling procedure. The electrostatic component of the Gibbs energy was calculated from a thermodynamic integration process with values of λ = 0.0, 0.1, 0.2, 0.3, 0.4, 0.5, 0.6, 0.7, 0.8, 0.9, and 1.0

$$U(\lambda) = (1 - \lambda)U_i + \lambda U_j \quad (7)$$

where U_i and U_j correspond to the states where the solvent−solute electrostatic interactions are completely on and completely off, respectively. The dispersion component of the Gibbs energy was calculated using an analogous decoupling scheme.

The repulsive component of the Gibbs energy was calculated from a staged free energy perturbation calculation where the repulsive component of the Lennard-Jones potential was scaled to zero in a continuous process. The details of this process are described in ref 72.

Each window of this perturbation was equilibrated for 1 ns and then sampled by a 3 ns simulation. The Gibbs energy of each component was calculated from these data using the weighted histogram analysis method (WHAM).[73]

Potential of Mean Force. The potential of mean force (PMF) for the dissolution of CH_3Br in liquid water was calculated by constructing a 2D slab of water with vacuum layers above and below it along the Z axis. The water slab had dimensions of 24 × 24 × 24 Å, containing 606 SWM4-NDP water molecules. The simulation cell had dimensions of 24 × 24 × 72 Å. A Langevin thermostat was used in these simulations, with friction coefficients of 5 and 10 ps^{-1} on the atomic and Drude masses, respectively. The water−vapor PMF was calculated by an umbrella sampling simulation where the center of mass of the CH_3Br solute was harmonically restrained at a series of distances from the center of mass of the water slab. The force constant of the harmonic restraint was 20.92 kJ mol^{-1} Å^{-2}. Simulations were performed in the interval Z = 0−32 Å at 1 Å increments. The potential of mean force for CH_3Br solvation was calculated from these simulations using the weighted histogram analysis method (WHAM).[74,75]

Diffusion Coefficient. The diffusion coefficient of bromomethane in water was calculated from MD simulations of a single CH_3Br molecule in a 32 × 32 × 32 Å box of SWM4-NDP water. After a 1 ns equilibration under NpT conditions, a 2.5 ns trajectory was sampled from a simulation under NVT conditions using a dual Nosé−Hoover thermostat.[76,77] The diffusion coefficient of CH_3Br was determined from the change in the RMSD of the solute over time via the Einstein equation

$$D_{PBC} = \frac{1}{6t}\langle |r_i(t) - r_i(0)|^2\rangle \quad (8)$$

DOI: 10.1021/acs.jpcb.5b09041
J. Phys. Chem. B 2015, 119, 13422−13432

The diffusion coefficient calculated using the Einstein model is corrected for periodic boundary conditions using the hydrodynamic correction of Yeh and Hummer[78]

$$D = D_{PBC} + 2.837297\frac{k_B T}{6\pi\eta L} \quad (9)$$

RESULTS AND DISCUSSION

Unmodified Nonpolarizable Models. The physical properties of liquid bromomethane were calculated using the GAFF, CGenFF, and OPLS force fields. These simulations were performed at the boiling point of bromomethane at standard pressure (T = 276 K). The Br nonbonded parameters and properties calculated using these models are presented in Table 1.

The densities calculated using the GAFF and CGenFF force fields are 4−5% lower than the experimental value of 1722 kg m^{-3}. The enthalpies of vaporization calculated using these models are also much lower than the experimental value of 24.1 kJ mol^{-1}. The OPLS model performs considerably better, predicting a density of 1732 kg m^{-3} and an enthalpy of vaporization of 24.99 kJ mol^{-1}. The surface tension calculated with the OPLS model also in closest agreement with experiment (23.6 dyn/cm calculated vs 27.7 dyn/cm experimentally). The GAFF and CGenFF models significantly underestimate the surface tension, with values of 17.3 and 18.1 dyn/cm, respectively.

The models are generally in reasonable agreement with the high-level ab initio (CCSD(T)/aug-cc-pVTZ//MP2/aug-cc-pVTZ) dimerization energy. The dimerization energy calculated using the GAFF force field is −10.7 kJ mol^{-1}, which is closest to the reference value of −10.3 kJ mol^{-1}. The CGenFF model underestimates the dimerization energy by 2.8 kJ mol^{-1}, while the OPLS model overestimates it by 2.2 kJ mol^{-1}. Notably, the GAFF model has a more accurate dimerization energy than the OPLS model but is far less accurate in the prediction of the physical properties, indicating that a more accurate dimerization energy does not imply that the model is generally superior.

The Br−Br, C−Br, and C−C radial distribution functions (RDFs) of bromomethane calculated from the AIMD and force field models are presented in Figure 1. Significant differences are apparent in the location of the first peak of the Br−Br RDF. In a simple liquid like bromomethane, this peak corresponds to the atomic diameter for Br. The Br−Br peak begins near r = 3.25 Å in the RDF calculated from the AIMD simulation. The force field models have significantly larger Br radii. The peak begins near r = 3.4 Å for the OPLS force field and r = 3.5 Å for the GAFF and CGenFF models. These anomalously large Br radii are consistent with the low liquid density predicted by the GAFF and CGenFF models. The location of the peak in the C−C RDFs are also overestimated by the GAFF and CGenFF models in comparison to the AIMD results.

The shapes of the RDFs are characteristic of a polar liquid. The peak in the Br−Br RDF corresponding to the first coordination sphere (3−6 Å) has two maxima. These maxima correspond to the contributions of the two major arrangements of CH_3Br contact pairs. The peak at 4 Å corresponds to parallel arrangements of neighboring molecules. The peak at 5.5 Å corresponds to arrangements where the molecules are aligned end-to-end.

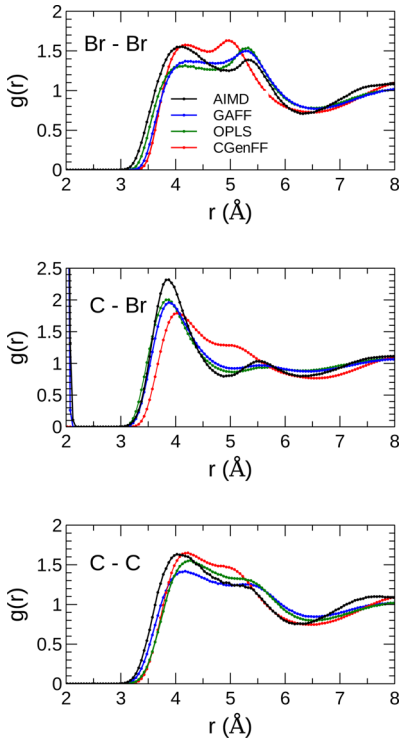

Figure 1. Br−Br, C−Br, and C−C RDFs of bromomethane at 276 K calculated from MD simulations using GAFF, CGenFF, and OPLS models. RDFs calculated from the AIMD simulation are shown for comparison (black).

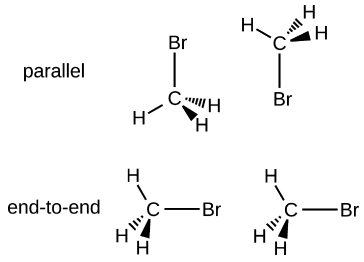

The first maximum in the AIMD Br−Br RDF is higher than the second, indicating that parallel configurations are more probable than end-to-end configurations. The OPLS and GAFF models reverse this ranking, predicting the end-to-end configurations to be more probable. This can be attributed to the anomalously high molecular dipole moments in these models (μ_0 = 2.17 and 2.52 D, respectively), which would favor the end-to-end configuration that maximizes the dipole−dipole interaction. The GAFF model has a high dipole moment because its charges are fit to the ESP surface calculated using HF/6-31G*, which tends to overestimate dipole moments.[84] This effect is attenuated in the CGenFF model, which has a low dipole moment (μ_0 = 1.402 D).

The poor performance of the GAFF and CGenFF models and the relative success of the OPLS model cannot be attributed to the molecular dipole moments alone because the dipole moment of the GAFF model is closer to the experimental value than is the dipole moment of the OPLS model. The Br Lennard-Jones parameters of the three models also vary dramatically. The most significant difference between the OPLS model and the other models is its significantly smaller Lennard-Jones radius for Br (σ_{Br} = 1.94747 Å), suggesting that this parameter is not optimal for bromo-

DOI: 10.1021/acs.jpcb.5b09041
J. Phys. Chem. B 2015, 119, 13422−13432

methane in the GAFF and CGenFF force fields. The Br−Br RDFs also indicate that the Br radii are too large in these models.

Reparameterization of the Lennard-Jones Parameters. In an attempt to improve the accuracy of the GAFF and CGenFF models, the Lennard-Jones parameters of the Br atom were reparameterized to reproduce the experimental density and enthalpy of vaporization at 276 K. The OPLS force field was not reparameterized because it was already nearly optimal.

Table 2. Parameters and Calculated Properties of Liquid Bromomethane (T = 276 K, p = 101.325 kPa) for the Reparameterized Nonpolarizable Models

property	GAFF (opt)	CGenFF (opt)	exptl
σ_{Br} (Å)	1.7061	1.6953	
ϵ_{Br} (kJ mol^{-1})	1.6531	2.1846	
q_{Br} (e)	−0.124661	−0.10	−0.22
μ_0 (D)	2.17	1.402	1.797 ± 0.015
E_{dimer} (kJ mol^{-1})	−11.0	−7.7	−10.3
ρ (kg m^{-3})	1722.8 ± 0.6	1723.94 ± 0.84	1722.0
ΔH_{vap} (kJ mol^{-1})	24.77 ± 0.04	23.85 ± 0.1	24.1
γ (dyn/cm)	12.5 ± 0.8	19.7 ± 0.4	27.3
ϵ	10.1 ± 0.1	4.93 ± 0.02	9.71

To identify the optimal parameters, an iterative grid search was performed on the Br Lennard-Jones σ and ϵ parameters with a resolution of $\sigma \pm 0.001$ Å and $\epsilon \pm 0.0418$ kJ mol^{-1}. A 1 ns NpT equilibration simulation followed by a 2 ns production simulation was performed to determine the properties of each putative set of parameters. The target function for the optimization was

$$\delta(\sigma, \varepsilon) = (\rho_{ref} - \rho_{calcd})^2 + (\Delta H_{vap,ref} - \Delta H_{vap,calcd})^2 \quad (10)$$

Parameters were identified for both models that give densities and enthalpies of vaporization in good agreement with experiment. The parameters and calculated properties are presented in Table 2. In each case, the Lennard-Jones radius of Br was significantly decreased from the radius defined in the original parameter set (GAFF, σ_{Br} = 1.7996 → 1.7061 Å; CGenFF, σ_{Br} = 1.7551 → 1.6953 Å). The reparameterization had only a small effect on the dimerization energies and dielectric constants. The surface tension calculated with the reparameterized GAFF model was in even poorer agreement with experiment (γ = 12.5 dyn/cm), while the CGenFF model was only slightly improved (γ = 19.7 dyn/cm).

The RDFs calculated from simulations using the new Lennard-Jones parameters were generally in better agreement with the AIMD RDFs (Figure 2). This was particularly true for the Br−Br RDF, where the first peaks now have very similar positions. The GAFF force field still predicts the second Br−Br peak to be larger, although that is likely due to the anomalously large molecular dipole moment (μ_0 = 2.17 D), which disfavors orientations with shorter Br−Br distances. This feature cannot be improved simply by reoptimizing the Lennard-Jones parameters. Generally, all three models are in fair agreement with the available experimental and AIMD data when the Br Lennard-Jones parameters are optimal.

Polarizable Model. To develop a model that provides a more accurate description of liquid bromomethane, we

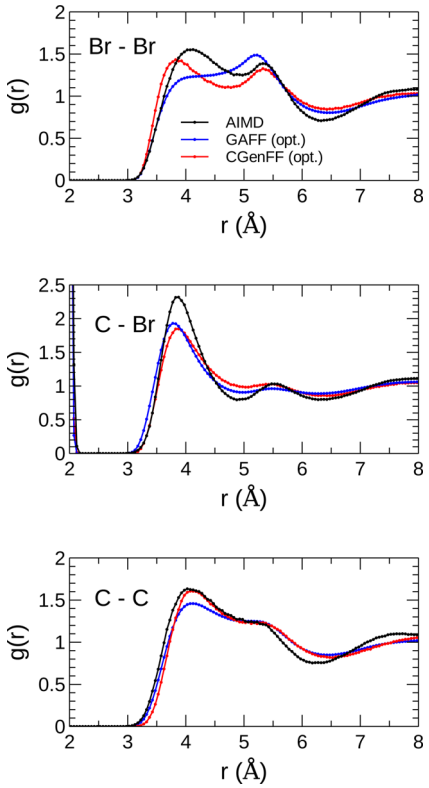

Figure 2. Br−Br, C−Br, and C−C RDFs of bromomethane at 276 K calculated from MD simulations using the reparameterized GAFF and CGenFF models. RDFs calculated from the AIMD simulation are shown for comparison (black).

parametrized a polarizable model following the Drude force field framework. To model the effect of the C−Br σ-hole, a lone-pair site was added collinear to the C−Br bond axis, 0.7 Å from the Br center. A schematic of this model is presented in Figure 3. This distance was selected because it provided the lowest RMSE in the charge-fitting step. The charges and polarizabilities were fit to the static and perturbed B3LYP/aug-cc-pVDZ electrostatic potential surfaces using the FITCHARGE module of CHARMM.[85] The calculated B3LYP/aug-cc-pVDZ dipole moment is 1.72 D, so the calculated charges were scaled so that the static dipole moment matched the experimental value of 1.80 D. A polarizability scaling factor of 0.7 was used.

This model was found to give good agreement to the target QM electrostatic potential on the static and perturbed arcs 2.5 Å from the Br atom (Figure 4). The perturbed surfaces were

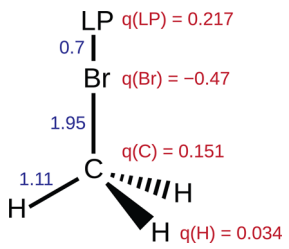

Figure 3. Schematic of the Drude model for bromomethane. Equilibrium bond lengths are given adjacent to the bonds in blue. Charges of the sites (q) are given in red. The lone-pair pseudoatom (LP) added to describe the σ-hole effect is located 0.7 Å along the C−Br bond axis, on the opposite face of the Br atom from the C atom.

DOI: 10.1021/acs.jpcb.5b09041
J. Phys. Chem. B 2015, 119, 13422−13432

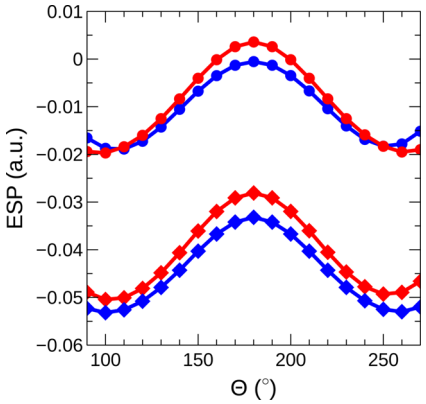

Figure 4. QM (blue) and Drude (red) MM ESP arcs around of Br atom of bromomethane at a distance of 2.5 Å. Static (unperturbed) ESPs are indicated by circles. Surfaces that are perturbed by a 0.5 e point charge at the given point on the arc are indicated by diamonds.

calculated by placing a point charge (q = 0.5 e) at the position along the arc the perturbed ESP is determined for. The Drude and QM unperturbed ESPs show a maximum at θ = 180°, consistent with a σ-hole. The effect of induced polarization is large, with the perturbed arcs roughly −0.03 au lower than the unperturbed ESPs.

Br Lennard-Jones parameters for the Drude force field had not been previously reported, so these parameters were determined by optimization. The initial parameters were generated by the GAMPP parametrization utility.[86] The Lennard-Jones parameters for Br were then reparameterized to reproduce the experimental enthalpy of vaporization and density by the same procedure that the nonpolarizable models were reparameterized. The calculated properties and parameters of the Drude model are presented in Table 3.

Table 3. Parameters and Calculated Properties of Liquid Bromomethane (T = 276 K, p = 101.325 kPa) for the Drude Polarizable Model

property	Drude	exptl
σ_{Br} (Å)	1.780	
ε_{Br} (kJ mol^{-1})	1.8916	
q_{Br} (e)	−0.470	
q_{LP} (e)	0.217	
μ_0 (D)	1.80	1.797 ± 0.015
E_{dimer} (kJ mol^{-1})	−10.6	−10.3
ρ (kg m^{-3})	1721.0 ± 0.5	1722
ΔH_{vap} (kJ mol^{-1})	24.2 ± 0.1	24.1
γ (dyn/cm)	20.7 ± 1.6	27.3
ϵ_0	14.0 ± 0.6	9.71

The optimal Lennard-Jones parameters were found to be σ_{Br} = 1.78 Å and ε_{Br} = 1.892 kJ mol^{-1}. This value of σ_{Br} is somewhat larger than the optimal parameters for the optimized nonpolarizable models, which ranged from 1.6953 to 1.734 Å.

Generally, the physical properties calculated using the Drude model are in fair agreement with the experimental values. The dielectric constant is overestimated, with a value of 14.0, in comparison to the experimental value of 9.71. The surface tension is 20.7 dyn/cm vs the experimental value of 27.7 dyn/cm. The dimerization energy is −10.6 kJ mol^{-1}, which is closest to the ab initio value of −10.3 kJ mol^{-1} of any of the models.

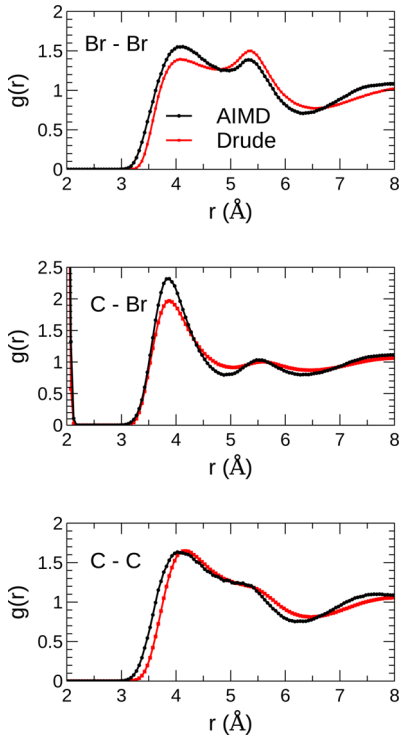

Figure 5. Br−Br, C−Br, and C−C RDFs of CH_3Br at 276 K calculated from MD simulations using the Drude and AIMD models.

The RDFs calculated using the Drude model agree well with the results from the AIMD simulation (Figure 5). The start of the first Br−Br peak occurs at a slightly larger distance in the Drude model than the AIMD model (r = 3.4 Å vs r = 3.35 Å), but the general shape of the peaks of the RDFs are consistent between the Drude and the AIMD models. The C−C RDF is also shifted to larger distances with respect to the AIMD curve. Improving this would require the reoptimization of the methyl carbon atom type parameters in the Drude polarizable force field. It should be noted that the AIMD curves are also inexact due to the limited size of the unit cell, relatively short simulation time, use of pseudopotentials, finite basis set, basis set superposition error, and use of an inexact exchange-correlation functional. Nevertheless, the strong agreement between the Drude and the AIMD simulations for the RDFs suggests that the more elaborate description of electrostatics in the Drude model results in a more accurate description of the liquid structure.

Although the dimerization energy, surface tension, and dielectric constant of the Drude model do not match the reference values exactly, the deviations are relatively modest. Nevertheless, this model is only incrementally more accurate than some of the nonpolarizable models (e.g., OPLS). This indicates that models that include polarizability and the σ-hole effect are not essential for describing most features of liquid bromomethane.

Solution Properties. *Solvation of Bromomethane in Liquid Water.* The Drude model developed in this study was used to simulate the solvation of bromomethane in liquid water (Figure 6). To test the accuracy of this model, the hydration free energy of bromomethane was calculated using FEP. The components of the solvation energy and total energies are collected in Table 4. The solvation energy predicted by the model is −5.6 kJ mol^{-1} vs the experimental value of −3.5 kJ

DOI: 10.1021/acs.jpcb.5b09041
J. Phys. Chem. B 2015, 119, 13422−13432

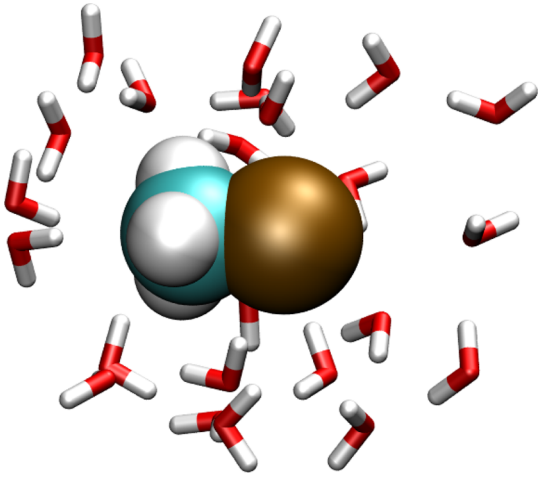

Figure 6. Representative configuration of the hydrated structure of bromomethane from an MD simulation of $CH_3Br(aq)$ using the Drude model.

mol^{-1}. Although the solubility of bromomethane is overestimated, it is correctly predicted to be a moderately soluble compound. For other molecules, it was necessary to define pairwise Lennard-Jones parameters to achieve subkcal accuracy in the calculated Gibbs energies of hydration.[7,87] Likewise, the diffusion coefficient of bromomethane in water at 19.4 °C calculated using this model is 2.09 ± 0.28 × 10^{-5} cm^2 s^{-1}, which is a moderate overestimate of the experimental value of 1.50 × 10^{-5} cm^2 s^{-1}.[88]

Table 4. Gibbs Energy of Hydration of Bromomethane Calculated Using the Drude Model[a]

ΔG°_{hydr}	calcd	exptl
electrostatic	−8.8	
dispersive	−38.0	
repulsive	41.2	
total	−5.6	−3.5

[a]All values are in kJ mol^{-1}. The experimental value is estimated from the solubility constant reported in ref 89. The standard state used is 1 M gas →1 M solution.

The components of the hydration energy show that solute−water dispersion interactions make a significantly larger contribution than electrostatic interactions do (ΔG_{disp} = −38.0 kJ mol^{-1} vs ΔG_{elec} = −8.8 kJ mol^{-1}). These two effects are countered by the large repulsive energy, corresponding to the thermodynamic cost of creating a cavity in the liquid (ΔG_{repul} = 41.2 kJ mol^{-1}). The dispersion and repulsive components effectively counter each other, but the modest electrostatic interactions are sufficient to impart modest solubility.

The Br−water distributions were calculated to determine the nature of the water−Br interactions (Figure 7). The Br−O RDF shows a broad peak centered at r_{Br-O} = 3.5 Å. The Br−H RDF shows a sharp but short peak at r_{Br-H} = 2.5 Å. This is generally indicative of the water acting as a hydrogen-bond donor to the Br. Integration of the C−Br···H peak shows that the Br atom generally accepts 2−3 hydrogen bonds from water molecules. Analysis of the C−Br···O and C−Br···H distance vs angle distribution functions shows that the most probable C−Br···water angles are in the 75−105° range (Figure 8). This is

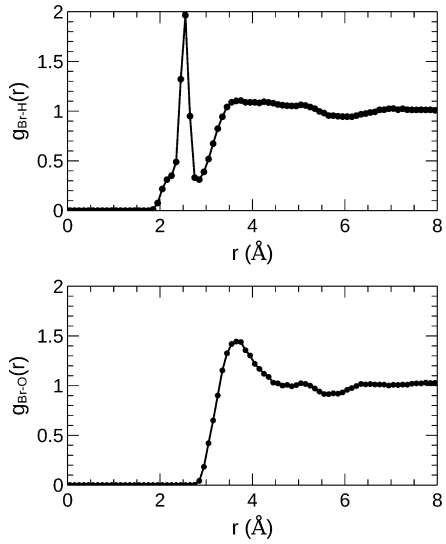

Figure 7. Radial distribution functions of bromomethane in water calculated using the Drude model. (Top) Br···H−OH distribution; (bottom) Br···OH_2 distribution.

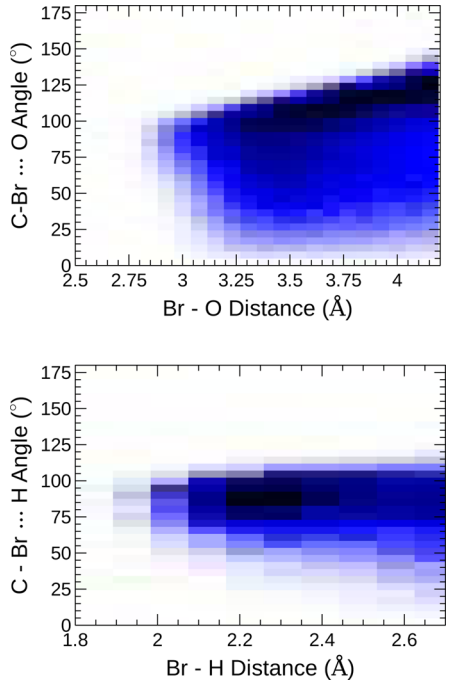

Figure 8. Probability distribution of the Br−OH_2 distances vs C−Br···OH_2 distances.

consistent with the Br atom acting as a hydrogen-bond acceptor on the sides orthogonal to the C−Br bond axis, where the electrostatic potential is most negative (Figure 4). A representative configuration of this hydration structure is presented in Figure 6.

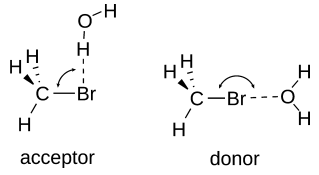

DOI: 10.1021/acs.jpcb.5b09041
J. Phys. Chem. B 2015, 119, 13422−13432

The C—Br···O distribution shows that the probability of an O atom of water molecule holding an angle near 180° is low. These orientations would correspond to a halogen-bond-type interaction with the negatively charged O atom of water via the σ-hole. The absence of these interactions indicates that bromomethane does not halogen bond with liquid water. The lack of halogen bonding is consistent with the static ESP surface, which is approximately zero at θ = 180°, so a Br···O(H_2) interaction would not be competitive to a water—water hydrogen-bonding interaction. This is consistent with quantum chemical analysis of CH_3Br—water interactions in the gas phase.[90]

Interfacial Properties. To investigate the hydration and interfacial properties of bromomethane, the Drude model was used to simulate the interaction of bromomethane with a model water—vapor interface. Figure 9 shows the potential of mean force (a.k.a. Gibbs energy profile) of a molecule of CH_3Br passing from a position in the gas phase (Z > 25 Å) into the bulk water phase at the center of a 2D slab of water (Z < 10 Å). The solute crosses the water—vapor interface in the Z = 10—20 Å range.

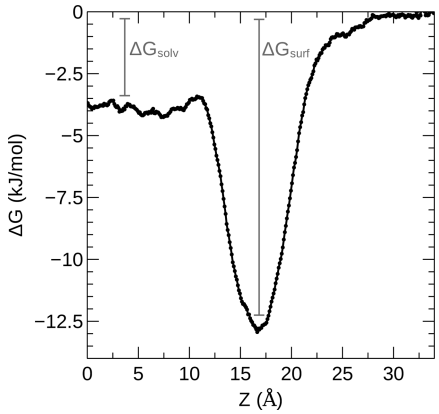

Figure 9. Potential of mean force (PMF) for the hydration of CH_3Br from the gas phase (Z > 25 Å) to bulk water (Z < 10 Å) through the water—vapor interface (10 Å < Z < 20 Å).

The PMF is consistent with the solvation and interfacial behavior of a sparingly soluble molecule. The PMF in the bulk water region averages between −3 and −4 kJ mol^{-1}, which is similar to the hydration energy calculated using FEP. There is a large surface excess, where the PMF in the interfacial region (12—24 Å) is 9 kJ mol^{-1} lower than in the bulk solvent (0—10 Å). From this PMF, we estimate that the Gibbs energy of a molecule of bromomethane absorbing to the surface of liquid water (ΔG_{surf}) is approximately −13 kJ mol^{-1}. This would result in a strong tendency for bromomethane molecules to partition to the interface, where they are preferentially oriented parallel to the water surface (Figure 10).

CONCLUSION

Three generalized force fields were evaluated for their abilities to predict the physical properties and liquid structure of bromomethane. The OPLS force field was reasonably accurate for the prediction of the density, enthalpy of vaporization, and surface tension of liquid bromomethane at 276 K. The default parameters for bromoalkanes in the GAFF and CGenFF force fields were generally unreliable. All of these models predicted

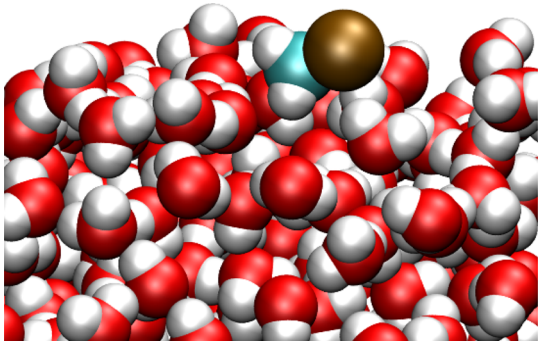

Figure 10. Representative configuration from the MD simulation of a CH_3Br molecule at the water—vapor interface using the Drude model.

significantly different radial distribution functions than those that were calculated using ab initio molecular dynamics.

The Lennard-Jones parameters for bromine in the GAFF and CGenFF models were reparameterized to reproduce the experimental density and enthalpy of vaporization of liquid bromomethane. The radial distribution functions calculated with these models were in better agreement with the AIMD simulations than the original parameters were. This suggests that the poor performance of these models can be addressed by simply optimizing the parameters of the Lennard-Jones potential and do not reflect a pathological failure due to the neglect of induced polarization or the σ-hole effect. Nevertheless, these models were not universally reliable for all properties that were examined; in some cases there were sizable errors for properties that were not part of the parametrization, like the dimerization energy, surface tension, and dielectric constant.

To develop a more accurate model for liquid bromomethane, a polarizable force field based on the Drude model was developed. A positively charged lone-pair site was added to the Br center to capture the effect of the C—Br σ-hole. Charges and polarizabilities were fit to the B3LYP/aug-cc-pVDZ ESP surfaces and constrained to reproduce the experimental static dipole moment. Lennard-Jones parameters for Br were optimized for this model. This model was in better agreement with the AIMD radial distribution function, and the physical properties calculated using this model were in similar or better agreement with experiment than the nonpolarizable models. This is the first reported Drude polarizable model of an organobromine compound.

This model was used to study the properties of aqueous and interfacial behavior of bromomethane. The hydration energy of this model was in reasonable agreement with experiment. Dispersion interactions were the dominant solvent—solute interaction, with electrostatic interactions also contributing to the moderate solubility of bromomethane. Bromomethane predominantly acts as a hydrogen-bond acceptor in aqueous solution, with water molecules forming hydrogen bonds with the Br atom perpendicular to the C—Br bond. The potential of mean force for the transition of bromomethane through the water—vacuum interface showed a significant surface excess, suggesting that bromomethane will concentrate at the interface.

This model is an example of how force fields can be parametrized for simple liquids where there is limited experimental data. The general strategy is to begin with a rigorous treatment of electrostatics by using a polarizable model with additional off-center charge sites to describe features like σ-holes. The atomic charges and polarizabilities are then fit to

DOI: 10.1021/acs.jpcb.5b09041
J. Phys. Chem. B 2015, 119, 13422—13432

perturbed electrostatic potential surfaces calculated using accurate quantum chemical methods (e.g., hybrid DFT). The Lennard-Jones parameters are then optimized to reproduce the bulk thermodynamic data that are available (e.g., density and enthalpy of vaporization). The liquid structure can then be validated by comparison to the structure calculated from an ab initio molecular dynamics simulation. Nevertheless, this model is not in perfect agreement with the reference data for properties like the dielectric constant and surface tension, indicating that a more elaborate force field would be needed to develop a universally accurate model. There are many further improvements that could be made to molecular mechanical force fields, including treatment of charge transfer effects,[91] the repulsive potential,[92] nonlinear polarizability effects,[93,94] and long-range dispersion.[95−97] Although fitting the electrostatic parameters to the QM ESP surfaces greatly simplifies the parametrization process, the high dielectric constant calculated with this model suggests this method of fitting could be refined further.

A positively charged lone-pair site collinear to the σ bond is an effective way to incorporate a σ-hole effect into a molecular mechanical model. Unfortunately, this type of site is not currently available in many simulation codes and charge-fitting programs. Further, most standard force fields have not been parametrized to include them. Generally, the Lennard-Jones parameters must be reoptimized if the electrostatic terms of a force field are changed, so including these features universally will be a significant undertaking. As the present example shows, rigorous parametrization of conventional nonpolarizable models is generally capable of providing good agreement with experimental physical properties of bulk liquids, even though these models neglect the effect of the σ-hole. QM data, such as ESP surfaces, high-level ab initio interaction energies, and AIMD trajectories, can provide additional data that can be used to parametrize models that include the σ-hole effect. The judicious introduction of off-center charge sites, incorporation of induced polarizability, and careful parametrization to experimental and QM data will allow the development of more reliable force fields that provide realistic models of organohalogen compounds.

■ ASSOCIATED CONTENT

Supporting Information

The Supporting Information is available free of charge on the ACS Publications website at DOI: 10.1021/acs.jpcb.5b09041.

Tabulated radial distribution functions, sample input files, topology, and parameter files (PDF)

■ AUTHOR INFORMATION

Corresponding Author

*E-mail: crowley@mun.ca.

Author Contributions

‡A.N.S.A., J.N.M., and T.T. contributed equally to this work.

Notes

The authors declare no competing financial interest.

■ ACKNOWLEDGMENTS

We thank the NSERC of Canada for funding through the Discovery Grant program (Application 418505-2012). A.A. thanks the Women in Science and Engineering Summer Student program. A.A., J.M., and T.T. thank the Canada Summer Jobs program. Computational resources were provided by Compute Canada (RAPI: djk-615-ab) through the Calcul Quebec, ACEnet, and Westgrid consortia.

■ REFERENCES

(1) Yang, R. S. H.; Witt, K. L.; Alden, C. J.; Cockerham, L. G. In *Reviews of Environmental Contamination and Toxicology*; Ware, G. W., Ed.; Reviews of Environmental Contamination and Toxicology; Springer: New York, 1995; Vol. *142*; pp 65−85.

(2) Mellouki, A.; Talukdar, R. K.; Schmoltner, A.-M.; Gierczak, T.; Mills, M. J.; Solomon, S.; Ravishankara, A. R. Atmospheric Lifetimes and Ozone Depletion Potentials of Methyl Bromide (CH_3Br) and Dibromomethane (CH_2Br_2). *Geophys. Res. Lett.* **1992**, *19*, 2059−2062.

(3) Anbar, A. D.; Yung, Y. L.; Chavez, F. P. Methyl Bromide: Ocean Sources: Ocean Sinks, and Climate Sensitivity. *Global Biogeochem. Cycles* **1996**, *10*, 175−190.

(4) Varner, R. K.; Crill, P. M.; Talbot, R. W. Wetlands: A Potentially Significant Source of Atmospheric Methyl Bromide and Methyl Chloride. *Geophys. Res. Lett.* **1999**, *26*, 2433−2435.

(5) Rhew, R. C.; Miller, B. R.; Weiss, R. F. *Nature* **2000**, *403*, 292−295.

(6) Yvon-Lewis, S. A.; Saltzman, E. S.; Montzka, S. A. Recent Trends in Atmospheric Methyl Bromide: Analysis of Post-Montreal Protocol variability. *Atmos. Chem. Phys.* **2009**, *9*, 5963−5974.

(7) Riahi, S.; Rowley, C. N. Solvation of Hydrogen Sulfide in Liquid Water and at the Water-Vapor Interface Using a Polarizable Force Field. *J. Phys. Chem. B* **2014**, *118*, 1373−1380.

(8) Jungwirth, P.; Tobias, D. J. Molecular Structure of Salt Solutions: A New View of the Interface with Implications for Heterogeneous Atmospheric Chemistry. *J. Phys. Chem. B* **2001**, *105*, 10468−10472.

(9) Vieceli, J.; Roeselová, M.; Potter, N.; Dang, L. X.; Garrett, B. C.; Tobias, D. J. Molecular Dynamics Simulations of Atmospheric Oxidants at the Air-Water Interface: Solvation and Accommodation of OH and O_3. *J. Phys. Chem. B* **2005**, *109*, 15876−15892.

(10) Vacha, R.; Jungwirth, P.; Chen, J.; Valsaraj, K. Adsorption of Polycyclic Aromatic Hydrocarbons at the Air-Water Interface: Molecular Dynamics Simulations and Experimental Atmospheric Observations. *Phys. Chem. Chem. Phys.* **2006**, *8*, 4461−4467.

(11) Girardet, C.; Toubin, C. Molecular Atmospheric Pollutant Adsorption on Ice: A Theoretical Survey. *Surf. Sci. Rep.* **2001**, *44*, 159−238.

(12) Wang, J.; Wolf, R. M.; Caldwell, J. W.; Kollman, P. A.; Case, D. A. Development and Testing of a General Amber Force Field. *J. Comput. Chem.* **2004**, *25*, 1157−1174.

(13) Jorgensen, W. L.; Tirado-Rives, J. Potential Energy Functions for Atomic-Level Simulations of Water and Organic and Biomolecular Systems. *Proc. Natl. Acad. Sci. U. S. A.* **2005**, *102*, 6665−6670.

(14) Vanommeslaeghe, K.; Hatcher, E.; Acharya, C.; Kundu, S.; Zhong, S.; Shim, J.; Darian, E.; Guvench, O.; Lopes, P.; Vorobyov, I.; et al. CHARMM General Force Field: A Force Field for Drug-like Molecules Compatible with the CHARMM All-Atom Additive Biological Force Fields. *J. Comput. Chem.* **2009**, *31*, 671−690.

(15) Caleman, C.; van Maaren, P. J.; Hong, M.; Hub, J. S.; Costa, L. T.; van der Spoel, D. Force Field Benchmark of Organic Liquids: Density, Enthalpy of Vaporization, Heat Capacities, Surface Tension, Isothermal Compressibility, Volumetric Expansion Coefficient, and Dielectric Constant. *J. Chem. Theory Comput.* **2012**, *8*, 61−74.

(16) Clark, T.; Hennemann, M.; Murray, J. S.; Politzer, P. Halogen Bonding: The σ-Hole. *J. Mol. Model.* **2007**, *13*, 291−296.

(17) Legon, A. C. The Halogen Bond: An Interim Perspective. *Phys. Chem. Chem. Phys.* **2010**, *12*, 7736−7747.

(18) Politzer, P.; Murray, J. S.; Concha, M. C. Halogen Bonding and the Design of New Materials: Organic Bromides, Chlorides and Perhaps Even Fluorides as Donors. *J. Mol. Model.* **2007**, *13*, 643−650.

(19) Voth, A. R.; Khuu, P.; Oishi, K.; Ho, P. S. Halogen Bonds as Orthogonal Molecular Interactions to Hydrogen Bonds. *Nat. Chem.* **2009**, *1*, 74−79.

(20) Metrangolo, P.; Meyer, F.; Pilati, T.; Resnati, G.; Terraneo, G. Halogen Bonding in Supramolecular Chemistry. *Angew. Chem., Int. Ed.* **2008**, *47*, 6114−6127.

DOI: 10.1021/acs.jpcb.5b09041
J. Phys. Chem. B 2015, 119, 13422−13432

(21) Gilday, L. C.; Robinson, S. W.; Barendt, T. A.; Langton, M. J.; Mullaney, B. R.; Beer, P. D. Halogen Bonding in Supramolecular Chemistry. *Chem. Rev.* **2015**, *115*, 7118−7195.
(22) Viger-Gravel, J.; Leclerc, S.; Korobkov, I.; Bryce, D. L. Direct Investigation of Halogen Bonds by Solid-State Multinuclear Magnetic Resonance Spectroscopy and Molecular Orbital Analysis. *J. Am. Chem. Soc.* **2014**, *136*, 6929−6942.
(23) Bogaard, M. P.; Buckingham, A. D.; Pierens, R. K.; White, A. H. Rayleigh Scattering Depolarization Ratio and Molecular Polarizability Anisotropy for Gases. *J. Chem. Soc., Faraday Trans. 1* **1978**, *74*, 3008−3015.
(24) Ibrahim, M. A. A. Molecular Mechanical Study of Halogen Bonding in Drug Discovery. *J. Comput. Chem.* **2011**, *32*, 2564−2574.
(25) Kolář, M.; Hobza, P. On Extension of the Current Biomolecular Empirical Force Field for the Description of Halogen Bonds. *J. Chem. Theory Comput.* **2012**, *8*, 1325−1333.
(26) Jorgensen, W. L.; Schyman, P. Treatment of Halogen Bonding in the OPLS-AA Force Field: Application to Potent Anti-HIV Agents. *J. Chem. Theory Comput.* **2012**, *8*, 3895−3901.
(27) Mu, X.; Wang, Q.; Wang, L.-P.; Fried, S. D.; Piquemal, J.-P.; Dalby, K. N.; Ren, P. Modeling Organochlorine Compounds and the σ-Hole Effect Using a Polarizable Multipole Force Field. *J. Phys. Chem. B* **2014**, *118*, 6456−6465.
(28) Lamoureux, G.; Roux, B. Modeling Induced Polarization with Classical Drude Oscillators: Theory and Molecular Dynamics Simulation Algorithm. *J. Chem. Phys.* **2003**, *119*, 3025−3039.
(29) Lopes, P.; Roux, B.; MacKerell, A. D., Jr. Molecular Modeling and Dynamics Studies with Explicit Inclusion of Electronic Polarizability: Theory and Applications. *Theor. Chem. Acc.* **2009**, *124*, 11−28.
(30) Lamoureux, G.; MacKerell, A. D., Jr.; Roux, B. A Simple Polarizable Model of Water Based on Classical Drude Oscillators. *J. Chem. Phys.* **2003**, *119*, 5185−5197.
(31) Lamoureux, G.; Harder, E.; Vorobyov, I. V.; Roux, B.; MacKerell, A. D., Jr. A Polarizable Model of Water for Molecular Dynamics Simulations of Biomolecules. *Chem. Phys. Lett.* **2006**, *418*, 245−249.
(32) Lamoureux, G.; Roux, B. Absolute Hydration Free Energy Scale for Alkali and Halide Ions Established from Simulations with a Polarizable Force Field. *J. Phys. Chem. B* **2006**, *110*, 3308−3322.
(33) Yu, H.; Whitfield, T. W.; Harder, E.; Lamoureux, G.; Vorobyov, I.; Anisimov, V. M.; MacKerell, A. D., Jr.; Roux, B. Simulating Monovalent and Divalent Ions in Aqueous Solution Using a Drude Polarizable Force Field. *J. Chem. Theory Comput.* **2010**, *6*, 774−786.
(34) Rowley, C. N.; Roux, B. The Solvation Structure of Na^+ and K^+ in Liquid Water Determined from High Level Ab Initio Molecular Dynamics Simulations. *J. Chem. Theory Comput.* **2012**, *8*, 3526−3535.
(35) Riahi, S.; Roux, B.; Rowley, C. N. QM/MM Molecular Dynamics Simulations of the Hydration of Mg(II) and Zn(II) Ions. *Can. J. Chem.* **2013**, *91*, 552−558.
(36) Harder, E.; Anisimov, V. M.; Whitfield, T.; MacKerell, A. D., Jr.; Roux, B. Understanding the Dielectric Properties of Liquid Amides from a Polarizable Force Field. *J. Phys. Chem. B* **2008**, *112*, 3509−3521.
(37) Vorobyov, I. V.; Anisimov, V. M.; MacKerell, A. D., Jr. polarizable Empirical Force Field for Alkanes Based on the Classical Drude Oscillator Model. *J. Phys. Chem. B* **2005**, *109*, 18988−18999.
(38) Zhu, X.; MacKerell, A. D., Jr. Polarizable Empirical Force Field for Sulfur-Containing Compounds Based on the Classical Drude Oscillator Model. *J. Comput. Chem.* **2010**, *31*, 2330−2341.
(39) Riahi, S.; Rowley, C. N. A Drude Polarizable Model for Liquid Hydrogen Sulfide. *J. Phys. Chem. B* **2013**, *117*, 5222−5229.
(40) Chowdhary, J.; Harder, E.; Lopes, P. E. M.; Huang, L.; MacKerell, A. D., Jr.; Roux, B. A Polarizable Force Field of Dipalmitoylphosphatidylcholine Based on the Classical Drude Model for Molecular Dynamics Simulations of Lipids. *J. Phys. Chem. B* **2013**, *117*, 9142−9160.
(41) Riahi, S.; Rowley, C. N. Why Can Hydrogen Sulfide Permeate Cell Membranes? *J. Am. Chem. Soc.* **2014**, *136*, 15111−15113.
(42) Patel, D. S.; He, X.; MacKerell, A. D., Jr. Polarizable Empirical Force Field for Hexopyranose Monosaccharides Based on the Classical Drude Oscillator. *J. Phys. Chem. B* **2015**, *119*, 637−652.
(43) Savelyev, A.; MacKerell, A. D., Jr. Balancing the Interactions of Ions, Water, and DNA in the Drude Polarizable Force Field. *J. Phys. Chem. B* **2014**, *118*, 6742−6757.
(44) Savelyev, A.; MacKerell, A. D., Jr. All-Atom Polarizable Force Field for DNA Based on the Classical Drude Oscillator Model. *J. Comput. Chem.* **2014**, *35*, 1219−1239.
(45) Savelyev, A.; MacKerell, A. D., Jr. Competition Among Li^+, Na^+, K^+, and Rb^+ Monovalent Ions for DNa in Molecular Dynamics Simulations Using the Additive CHARMM36 and Drude Polarizable Force Fields. *J. Phys. Chem. B* **2015**, *119*, 4428−4440.
(46) Baker, C. M.; Anisimov, V. M.; MacKerell, A. D., Jr. Development of CHARMM Polarizable Force Field for Nucleic Acid Bases Based on the Classical Drude Oscillator Model. *J. Phys. Chem. B* **2011**, *115*, 580−596.
(47) Lopes, P. E. M.; Huang, J.; Shim, J.; Luo, Y.; Li, H.; Roux, B.; MacKerell, A. D., Jr. Polarizable Force Field for Peptides and Proteins Based on the Classical Drude Oscillator. *J. Chem. Theory Comput.* **2013**, *9*, 5430−5449.
(48) Marx, D.; Hutter, J. *Ab Initio Molecular Dynamics*; Cambridge University Press: Cambridge, 2009.
(49) Vanommeslaeghe, K.; Hatcher, E.; Acharya, C.; Kundu, S.; Zhong, S.; Shim, J.; Darian, E.; Guvench, O.; Lopes, P.; Vorobyov, I.; et al. CHARMM General Force Field: A Force Field for Drug-like Molecules Compatible with the CHARMM All-Atom Additive Biological Force Fields. *J. Comput. Chem.* **2009**, *31*, 671−690.
(50) Yesselman, J. D.; Price, D. J.; Knight, J. L.; Brooks, C. L. MATCH: An Atom-Typing Toolset for Molecular Mechanics Force Fields. *J. Comput. Chem.* **2012**, *33*, 189−202.
(51) Lopes, P.; Roux, B.; MacKerell, A. D., Jr. Molecular Modeling and Dynamics Studies with Explicit Inclusion of Electronic Polarizability: Theory and Applications. *Theor. Chem. Acc.* **2009**, *124*, 11−28.
(52) Lopes, P. E. M.; Lamoureux, G.; Roux, B.; MacKerell, A. D., Jr. Polarizable Empirical Force Field for Aromatic Compounds Based on the Classical Drude Oscillator. *J. Phys. Chem. B* **2007**, *111*, 2873−2885.
(53) Lorentz, H. A. Ueber Die. Ueber Die Anwendung Des Satzes Vom Virial in Der Kinetischen Theorie Der Gase. *Ann. Phys. (Berlin, Ger.)* **1881**, *248*, 127−136.
(54) Berthelot, D. Sur. Le Mélange Des Gaz. *Compt. Rendus* **1898**, *126*, 1703−1706.
(55) Phillips, J. C.; Braun, R.; Wang, W.; Gumbart, J.; Tajkhorshid, E.; Villa, E.; Chipot, C.; Skeel, R. D.; Kalé, L.; Schulten, K. Scalable Molecular Dynamics with NAMD. *J. Comput. Chem.* **2005**, *26*, 1781−1802.
(56) Brooks, B. R.; Brooks, I. C. L.; MacKerell, A. D., Jr.; Nilsson, L.; Petrella, R. J.; Roux, B.; Won, Y.; Archontis, G.; Bartels, C.; Boresch, S.; et al. CHARMM: The Biomolecular Simulation Program. *J. Comput. Chem.* **2009**, *30*, 1545−1614.
(57) Darden, T.; York, D.; Pedersen, L. Particle Mesh Ewald: An N·Log(N) Method for Ewald Sums in Large Systems. *J. Chem. Phys.* **1993**, *98*, 10089−10092.
(58) Ryckaert, J.-P.; Ciccotti, G.; Berendsen, H. J. Numerical Integration of the Cartesian Equations of Motion of a System with Constraints: Molecular Dynamics of N-Alkanes. *J. Comput. Phys.* **1977**, *23*, 327−341.
(59) Feller, S. E.; Zhang, Y.; Pastor, R. W.; Brooks, B. R. Constant Pressure Molecular Dynamics Simulation: The Langevin Piston Method. *J. Chem. Phys.* **1995**, *103*, 4613−4621.
(60) Martyna, G. J.; Tobias, D. J.; Klein, M. L. Constant Pressure Molecular Dynamics Algorithms. *J. Chem. Phys.* **1994**, *101*, 4177−4189.
(61) VandeVondele, J.; Krack, M.; Mohamed, F.; Parrinello, M.; Chassaing, T.; Hutter, J. Quickstep: Fast and Accurate Density Functional Calculations Using a Mixed Gaussian and Plane Waves Approach. *Comput. Phys. Commun.* **2005**, *167*, 103−128.

DOI: 10.1021/acs.jpcb.5b09041
J. Phys. Chem. B 2015, 119, 13422−13432

(62) Perdew, J. P.; Burke, K.; Ernzerhof, M. Generalized Gradient Approximation Made Simple. *Phys. Rev. Lett.* **1996**, *77*, 3865−3868.
(63) Grimme, S.; Antony, J.; Ehrlich, S.; Krieg, H. A Consistent and Accurate Ab Initio Parametrization of Density Functional Dispersion Correction (DFT-D) for the 94 Elements H-Pu. *J. Chem. Phys.* **2010**, *132*, 154104.
(64) Krack, M. Pseudopotentials for H to Kr Optimized for Gradient-Corrected Exchange-Correlation Functionals. *Theor. Chem. Acc.* **2005**, *114*, 145−152.
(65) Boys, S.; Bernardi, F. The Calculation of Small Molecular Interactions by the Differences of Separate Total Energies. Some Procedures with Reduced Errors. *Mol. Phys.* **1970**, *19*, 553−566.
(66) Frisch, M. J.; Trucks, G. W.; Schlegel, H. B.; Scuseria, G. E.; Robb, M. A.; Cheeseman, J. R.; Scalmani, G.; Barone, V.; Mennucci, B.; Petersson, G. A.; et al. *Gaussian 09*, Revision D.01; Gaussian Inc.: Wallingford, CT, 2009.
(67) *TURBOMOLE V7.0 2015, a Development of University of Karlsruhe and Forschungszentrum Karlsruhe GmbH, 1989−2007*; TURBOMOLE GmbH, 2015; available from http://www.turbomole.com.
(68) Hättig, C.; Weigend, F. CC2 Excitation Energy Calculations on Large Molecules Using the Resolution of the Identity Approximation. *J. Chem. Phys.* **2000**, *113*, 5154−5161.
(69) Woon, D. E.; Dunning, T. H. Gaussian Basis Sets for Use in Correlated Molecular Calculations. III. the Atoms Aluminum Through Argon. *J. Chem. Phys.* **1993**, *98*, 1358−1371.
(70) *Liquefy VMD Plugin*; https://github.com/RowleyGroup/Liquefy (accessed Sept 25,2014).
(71) Neumann, M.; Steinhauser, O. Computer Simulation and the Dielectric Constant of Polarizable Polar Systems. *Chem. Phys. Lett.* **1984**, *106*, 563−569.
(72) Deng, Y.; Roux, B. Hydration of Amino Acid Side Chains: Nonpolar and Electrostatic Contributions Calculated from Staged Molecular Dynamics Free Energy Simulations with Explicit Water Molecules. *J. Phys. Chem. B* **2004**, *108*, 16567−16576.
(73) Kumar, S.; Rosenberg, J. M.; Bouzida, D.; Swendsen, R. H.; Kollman, P. A. The Weighted Histogram Analysis Method for Free-Energy Calculations on Biomolecules. I. The Method. *J. Comput. Chem.* **1992**, *13*, 1011−1021.
(74) Kumar, S.; Rosenberg, J. M.; Bouzida, D.; Swendsen, R. H.; Kollman, P. A. THE Weighted Histogram Analysis Method for Free-Energy Calculations on Biomolecules. I. the Method. *J. Comput. Chem.* **1992**, *13*, 1011−1021.
(75) Roux, B. The Calculation of the Potential of Mean Force Using Computer Simulations. *Comput. Phys. Commun.* **1995**, *91*, 275−282.
(76) Nosé, S. A. Unified Formulation of the Constant Temperature Molecular Dynamics Methods. *J. Chem. Phys.* **1984**, *81*, 511−519.
(77) Hoover, W. G. Canonical Dynamics: Equilibrium Phase-Space Distributions. *Phys. Rev. A: At., Mol., Opt. Phys.* **1985**, *31*, 1695−1697.
(78) Yeh, I.-C.; Hummer, G. System-Size Dependence of Diffusion Coefficients and Viscosities from Molecular Dynamics Simulations with Periodic Boundary Conditions. *J. Phys. Chem. B* **2004**, *108*, 15873−15879.
(79) Shulman, R. G.; Dailey, B. P.; Townes, C. H. Molecular Dipole Moments and Stark Effects. III. Dipole Moment Determinations. *Phys. Rev.* **1950**, *78*, 145−148.
(80) Frenkel, M.; Hong, X.; Dong, Q.; Yan, X.; Chirico, R. D. In *Densities of Halohydrocarbons*; Frenkel, M., Marsh, K. N., Eds.; Springer: Berlin/Heidelberg, 2003; Vol. *8J*.
(81) Riddick, J.; Bunger, W.; Sakano, T. *Organic Solvents: Physical Properties and Methods of Purification*, 4th ed.; John Wiley and Sons: New York, 1986.
(82) Yaws, C. L.; Richmond, P. C. In *Thermophysical Properties of Chemicals and Hydrocarbons*; Yaws, C. L., Ed.; William Andrew Publishing: Norwich, NY, 2009; pp 686−781.
(83) Morgan, S. O.; Lowry, H. H. Dielectric Polarization of Some Pure Organic Compounds in the Dissolved, Liquid, and Solid States. *J. Phys. Chem.* **1929**, *34*, 2385−2432.
(84) Hickey, A. L.; Rowley, C. N. Benchmarking Quantum Chemical Methods for the Calculation of Molecular Dipole Moments and Polarizabilities. *J. Phys. Chem. A* **2014**, *118*, 3678−3687.
(85) Anisimov, V. M.; Lamoureux, G.; Vorobyov, I. V.; Huang, N.; Roux, B.; MacKerell, A. D., Jr. Determination of Electrostatic Parameters for a Polarizable Force Field Based on the Classical Drude Oscillator. *J. Chem. Theory Comput.* **2005**, *1*, 153−168.
(86) Huang, L.; Roux, B. Automated Force Field Parameterization for Nonpolarizable and Polarizable Atomic Models Based on Ab Initio Target Data. *J. Chem. Theory Comput.* **2013**, *9*, 3543−3556.
(87) Baker, C. M.; Lopes, P. E. M.; Zhu, X.; Roux, B.; MacKerell, A. D., Jr. Accurate Calculation of Hydration Free Energies Using Pair-Specific Lennard-Jones Parameters in the CHARMM Drude Polarizable Force Field. *J. Chem. Theory Comput.* **2010**, *6*, 1181−1198.
(88) De Bruyn, W. J.; Saltzman, E. S. Diffusivity of Methyl Bromide in Water. *Mar. Chem.* **1997**, *57*, 55−59.
(89) De Bruyn, W. J.; Saltzman, E. S. the Solubility of Methyl Bromide in Pure Water, 35%. Sodium Chloride and Seawater. *Mar. Chem.* **1997**, *56*, 51−57.
(90) Wang, W.; Tian, A.; Wong, N.-B. Theoretical Study on the Bromomethane-Water 1:2 Complexes. *J. Phys. Chem. A* **2005**, *109*, 8035−8040.
(91) Stern, H. A.; Rittner, F.; Berne, B. J.; Friesner, R. A. Combined Fluctuating Charge and Polarizable Dipole Models: Application to a Five-Site Water Potential Function. *J. Chem. Phys.* **2001**, *115*, 2237−2251.
(92) Fanourgakis, G. S.; Xantheas, S. S. Development of Transferable Interaction Potentials for Water. V. Extension of the Flexible, Polarizable, Thole-Type Model Potential (TTM3-F, V. 3.0) to Describe the Vibrational Spectra of Water Clusters and Liquid Water. *J. Chem. Phys.* **2008**, *128*, 074506.
(93) Luo, Y.; Jiang, W.; Yu, H.; MacKerell, A. D., Jr.; Roux, B. Simulation Study of Ion Pairing in Concentrated Aqueous Salt Solutions with a Polarizable Force Field. *Faraday Discuss.* **2013**, *160*, 135−149.
(94) Yu, H.; Whitfield, T. W.; Harder, E.; Lamoureux, G.; Vorobyov, I.; Anisimov, V. M.; MacKerell, A. D., Jr.; Roux, B. Simulating Monovalent and Divalent Ions in Aqueous Solution Using a Drude Polarizable Force Field. *J. Chem. Theory Comput.* **2010**, *6*, 774−786.
(95) Fischer, N. M.; van Maaren, P. J.; Ditz, J. C.; Yildirim, A.; van der Spoel, D. Properties of Organic Liquids When Simulated with Long-Range Lennard-Jones Interactions. *J. Chem. Theory Comput.* **2015**, *11*, 2938−2944.
(96) Shirts, M. R.; Mobley, D. L.; Chodera, J. D.; Pande, V. S. Accurate and Efficient Corrections for Missing Dispersion Interactions in Molecular Simulations. *J. Phys. Chem. B* **2007**, *111*, 13052−13063.
(97) Isele-Holder, R. E.; Mitchell, W.; Hammond, J. R.; Kohlmeyer, A.; Ismail, A. E. Reconsidering Dispersion Potentials: Reduced Cutoffs in Mesh-Based Ewald Solvers Can Be Faster Than Truncation. *J. Chem. Theory Comput.* **2013**, *9*, 5412−5420.

DOI: 10.1021/acs.jpcb.5b09041
J. Phys. Chem. B 2015, 119, 13422−13432